Pergamon

Journal of Structural Geology, Vol. 18, No. 8, pp. 1031 to 1042, 1996

PII: S0191-8141(96)00032-6
0191-8141/96 $15.00 + 0.00

Structural permeability of fluid-driven fault–fracture meshes

RICHARD H. SIBSON

Department of Geology, University of Otago, P.O. Box 56, Dunedin, New Zealand

(*Received* 27 *June* 1995; *accepted in revised form* 26 *March* 1996)

Abstract—Fluid redistribution in the crust is influenced by hydraulic gradient, by existing permeability anisotropy arising from bedding and other forms of layering, and by structural permeability developed under the prevailing stress field. Field evidence suggests that mesh structures, comprising faults interlinked with extensional-shear and purely extensional vein-fractures, form important conduits for large volume flow of hydrothermal and hydrocarbon fluids. Meshes may be 'self-generated' by the infiltration of pressurised fluids into a stressed heterogeneous rock mass with varying material properties, developing best where bulk coaxial strain is symmetric with existing layering, but they also form under predominantly simple shear. Fluid passage through such structures generates earthquake swarm activity by distributed fault-valve action along suprahydrostatic gradients that may arise from compaction overpressuring, metamorphic dewatering, magmatic intrusion, and mantle degassing.

Within mesh structures, strong directional permeability may develop in the σ_2 direction parallel to fault–fracture intersections and orthogonal to fault slip vectors. In particular tectonic settings, this promotes strongly focused flow with high potential for mineralisation. Mesh activation requires the condition $P_f \sim \sigma_3$ to be maintained for the structures to remain high permeability conduits, requiring fluid overpressuring at other than shallow depths in extensional–transtensional regimes. Favoured localities for mesh development include linkage structures along large-displacement fault zones such as dilational jogs, lateral ramps, and transfer faults. In some circumstances, mesh formation appears to precede the development of major faults. Copyright © 1996 Elsevier Science Ltd

INTRODUCTION

The importance of fault-related fracture systems as host structures for hydrothermal mineralisation has long been recognised (Newhouse 1942, McKinstry 1948). Large volume fluid flow through an extensive rock volume is needed to form disseminated hydrothermal deposits of economic significance; for instance, given the low solubility of gold transported as complexes (~ 10 ppb), a flow of ~ 1 km^3 of aqueous fluid is needed to precipitate 10 tonnes of gold in a modest-sized deposit. However, while it is clear that fault–fracture networks form the principal avenues for large volume fluid flow in many areas, it is also notable that the hosting structures are generally not large displacement features. Here, we consider the factors which allow the development of extensive low-displacement fault–fracture networks and the flow of large fluid volumes, drawing comparisons with the distributed faulting and fracturing and accompanying fluid redistribution believed responsible for earthquake swarms.

EARTHQUAKE SWARMS AND FLUID REDISTRIBUTION

Earthquake swarms are a variant of seismic activity where a large number of small earthquakes occur throughout a substantial volume of rock with the activity waxing and waning through time, often without the occurrence of a distinct principal shock (Sykes 1970). Recorded swarm earthquakes are commonly in the microearthquake range ($1 < \mathbf{M} < 3$) with slip increments of millimetres to centimetres associated, respectively, with individual rupture dimensions of tens to hundreds of metres (Sibson 1989). Smaller events may, however, go undetected. The predominance of small earthquakes over large means that swarms sometimes have rather high b-values in comparison with 'normal' tectonic seismicity. Swarm activity may remain more or less stationary in space (e.g. Danville, California (Lee *et al.* 1971)) but may also be migratory with the locus of activity changing with time (e.g. swarms in the Taupo Volcanic Zone, New Zealand (Grindley & Hull 1986)).

Earthquake swarms are most frequently associated with areas of recent volcanic or geothermal activity within extensional and transtensional tectonic regimes; in the latter case, they tend to be localized within dilational jogs along strike-slip faults (Weaver & Hill 1979). Less commonly, swarms have been described from areas of active compressional tectonics such as the Santa Barbara Channel, California (Shaw & Suppe 1994). Swarm activity has been attributed either to high levels of material and/or stress heterogeneity within the rock mass (Mogi 1963, Scholz 1968) or, on the basis of tectonic setting, to the migration of magmatic and/or hydrothermal fluids (e.g. Sykes 1970, Hill 1977, Gold & Soter 1985).

Hill (1977) mesh model for earthquake swarms

To account for the volumetric character of earthquake swarms, the preponderance of small earthquakes over large, and their common association with volcanic/geothermal areas, Hill (1977) proposed a mechanical model for swarms involving the migration of fluids through a 'honeycomb' mesh of interlinked minor shear fractures (faults) and extension fractures (Fig. 1). Termination of individual shears in extension fractures inhibits the development of large throughgoing faults and

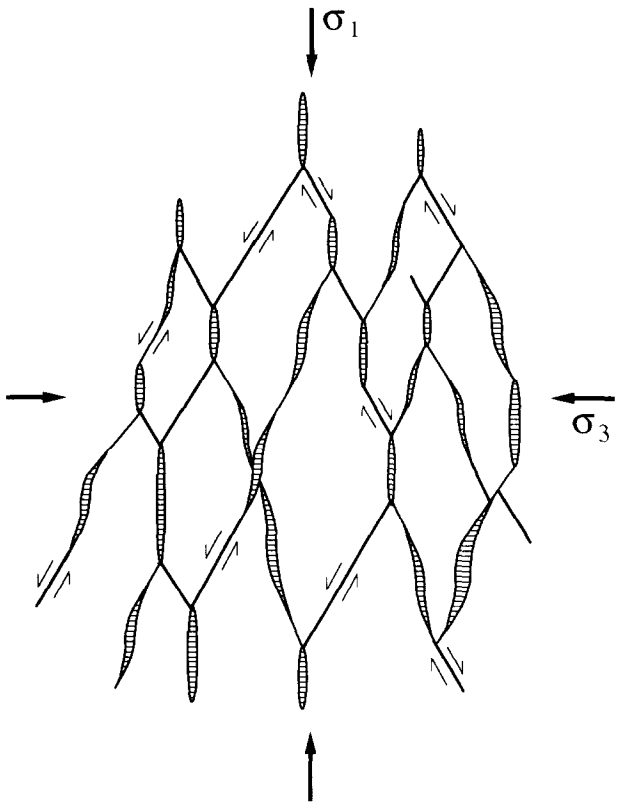

Fig. 1. Hill (1977) mesh model for earthquake swarms comprising interlinked shear, extensional, and extensional-shear fractures developed in a triaxial stress field. Diagram represents an extensional normal-fault stress regime when upright, a compressional thrust-fault regime when viewed sideways, and a strike-slip regime in plan view.

accounts for the dominance of small ruptures. Hill invoked igneous intrusion as the primary driving force for swarm activity, with dykes intruding a set of *en echelon* extension fractures linked by crack-tip shears. However, noting the occurrence of swarm-like seismicity induced by artificial fluid injection at Denver and Rangeley, Colorado (Healy *et al.* 1968, Raleigh *et al.* 1976), he also suggested that earthquake swarm activity might be triggered by the migration of hydrothermal fluids through similar fault–fracture meshes.

The Matsushiro earthquake swarm

The earthquake swarm that occurred from 1965 to 1967 near Matsushiro in Central Honshu, Japan (Fig. 2), is an example of particularly intense swarm activity accompanied by the development of laterally extensive strike-slip faulting and significant fluid redistribution. Over 700,000 shocks ranging up to **M**5 were recorded, the whole being energetically equivalent to one ~**M**6.3 earthquake (Hagiwara & Iwata 1968). Most of the activity occurred within an ellipsoidal volume (dimensions ~34 km NE–SW, by ~18 km NW–SE, by ~8 km deep) centred around Mt Minakami, a Quaternary andesitic lava dome. Three peaks in swarm activity occurred in the periods November–December 1965, March–April 1966 and August–September 1966, the last two being very pronounced (> 500 felt earthquakes per day).

Despite strong NE–SW elongation of the swarm along a well-defined structural grain, surface deformation in the form of a mesh structure of *en echelon* tension crack shear zones developed during the third peak in swarm activity to define a NW–SE trending left-lateral fault zone, some 500 m in width, which could be traced for over 5 km (Tsuneishi & Nakamura 1970). The deformation included vertical left-lateral shear zones oriented WNW–ESE to E–W and right-lateral shear zones oriented NE–SW to ENE–WSW (Fig. 2). Geodetic measurements showed that a total left-slip of ~0.5 m accompanied by ~0.3 m of NE–SW extension occurred across the main fault zone, consistent with focal mechanism analyses which yielded double-couple solutions involving either left-lateral strike-slip along steep NW–SE planes, or dextral strike-slip along NE–SW planes (Ichikawa 1969). The various observations are consistent with the activation under E–W compression of a Hill-type strike-

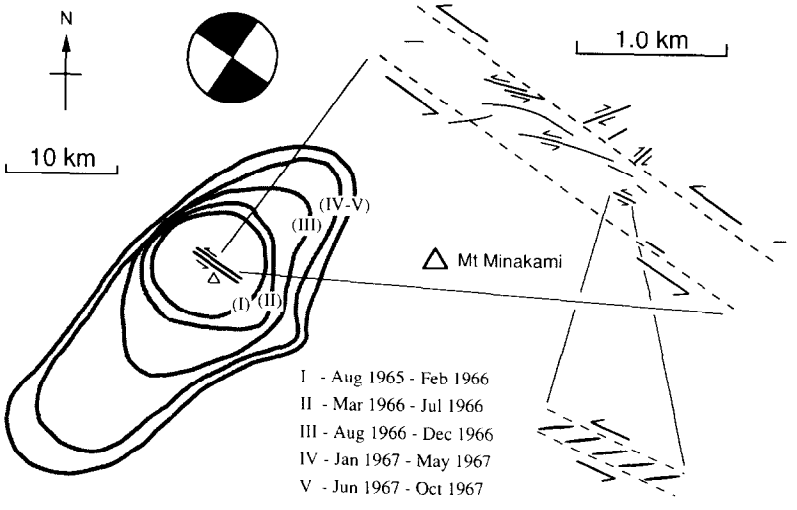

Fig. 2. Time-dependent development of the 1965–67 Matsushiro earthquake swarm and associated surface deformation with composite strike-slip focal mechanism (after Hagiwara & Iwata 1968, Ichikawa 1969, Tsuneishi & Nakamura 1970).

slip fault–fracture mesh extending throughout the entire focal volume.

Swarm development was accompanied by doming of the epicentral area to a maximum of over 0.8 m during the third peak of seismic activity, after which some subsidence occurred. Spring flow in the epicentral area increased markedly following the two latter peaks in swarm activity and, immediately after the third peak, a large volume ($<10^7$ m^3) of warm Na–Ca–chloride brine saturated with CO_2 was discharged from the area of ground fissuring (Morimoto *et al.* 1967, Tsuneishi & Nakamura 1970). Following the outpouring, seismicity diminished in what previously had been one of the most intensely active areas. Subsequent studies have shown abnormally high $^3He/^4He$ ratios, possibly derived from a shallow magmatic intrusion, to be present in soil gases within the main shear zone (Wakita *et al.* 1978).

Explanations put forward to account for the Matsushiro phenomena include stress-driven prefailure dilatancy and fluid diffusion around the developing fault zone with postfailure recovery leading to fluid expulsion (Nur 1974, Kisslinger 1975), or an episode of magmatic intrusion at depth (Stuart & Johnston 1975, Wakita *et al.* 1978). Nakamura (1971), however, suggested, that the primary cause of the Matsushiro swarm and its accompanying effects was the vertical migration of a package of overpressured hydrothermal fluid (a 'water eruption'), a view latterly supported by Mogi (1988). Irrespective of magmatic involvement, the Matsushiro swarm clearly represents a case of swarm seismicity linked to a major episode of hydrothermal fluid migration through a laterally extensive strike-slip fault–fracture mesh. Similar but less well documented episodes of fluid effusion have been noted accompanying swarm activity along the belt of normal faults within the Taupo Volcanic Zone in the North Island of New Zealand (Grindley & Hull 1986).

DEVELOPMENT OF FAULT–FRACTURE MESHES

Fluid migration through the crust is influenced by 3-D interconnections between existing discontinuities such as bedding, joints, faults, foliation, igneous contacts, etc. Because of crustal heterogeneity with material properties varying widely over a range of scales, particularly in areas of structural overprinting, the local stress state which affects the aperture of existing discontinuities may show considerable variation from the far-field stress (Fig. 3). As a consequence, the permeability structure is also likely to be highly heterogeneous. The hypothesis advanced here is that infiltration of pressurised fluids into stressed heterogeneous crust, perhaps initially along existing discontinuities, may induce a range of differently oriented brittle structures that become progressively interlinked into a structural mesh which adds to the permeability of the rock mass. Evidence that such mesh structures are primarily fluid-driven comes from their localisation within often uniform rock masses, from hydrothermal alteration and veining indicating their role as fluid

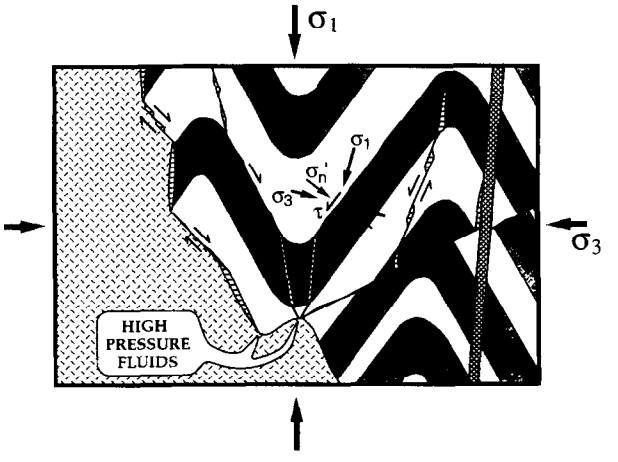

Fig. 3. Schematic illustration of the inception of a fault–fracture mesh as a consequence of pressurised fluid infiltration into stressed heterogeneous crust with inherited structure. Material heterogeneity causes local departures from the far-field stress and varying modes of brittle failure.

conduits, and from the presence of extension veins indicative of local overpressuring. The resulting bulk structural permeability within the rock mass can thus be regarded as 'self-generated' by the infiltrating fluids.

Stress controls on structural permeability

In a fluid-saturated rock mass, all normal stresses are reduced by the fluid pressure, P_f, to give effective stresses, $\sigma_n' = (\sigma_n - P_f)$ (Hubbert & Rubey 1959). The effective principal compressive stresses are then $\sigma_1' = (\sigma_1 - P_f) > \sigma_2' = (\sigma_2 - P_f) > \sigma_3' = (\sigma_3 - P_f)$, and the orientation, with respect to the triaxial stress field, of structural elements formed by different modes of brittle failure in intact, homogeneous and isotropic rock is reasonably described by classical failure theory involving a composite Griffith–Coulomb failure envelope (Fig. 4) (e.g. Brace 1960, Hancock 1985). Different stress-controlled structural elements affecting rock mass permeability are listed in Table 1, along with appropriate macroscopic failure criteria expressed in terms of the fluid pressure condition for failure. For intact rock, they include: (i)

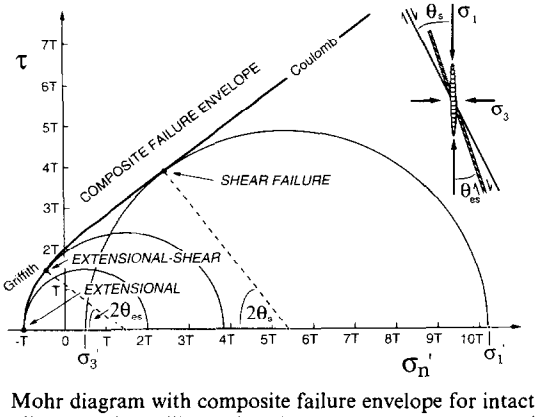

Fig. 4. Mohr diagram with composite failure envelope for intact rock with tensile strength, T, illustrating the stress conditions and orientations with respect to the stress field of: (a) extensional failure; (b) hybrid extensional-shear failure; and, (c) compressional shear failure, for a particular rock-type.

Table 1. Stress-control of fault–fracture mesh components. Fluid-pressure criteria for different varieties of macroscopic brittle failure are expressed in terms of rock material properties (tensile strength, T; cohesive strength, $C_i \sim 2T$; and internal coefficient of rock friction, μ_i, for intact rock; cohesive strength, C_e, and static friction coefficient, μ_s, along an existing plane of weakness) after Secor (1965) and Etheridge (1983)

Type of failure	Orientation	Criterion	Conditions
Grain-scale microcracks	$\sim \perp r\,\sigma_3$	—	grain impingement
Hydraulic extension fractures	$\perp r\,\sigma_3$	$P_f = \sigma_3 + T$	$(\sigma_1 - \sigma_3) < 4T$
Extensional shear fractures (Griffith criterion)	plane containing σ_2 at $0 < \theta < \theta_i\,\sigma o$	$P_f = \sigma_n + \dfrac{(4T^2 - \tau^2)}{4T}$	$4T < (\sigma_1 - \sigma_3) < 6T$
Shear fractures or faults (Coulomb criterion)	plane containing σ_2 at $20 < \theta_i < 30°$ to σ_1	$P_f = \sigma_n + \dfrac{(2T - \tau)}{\mu_i}$	$(\sigma_1 - \sigma_3) > 6T$
Shear reactivation of existing planes with cohesion, C_e	planes not orthogonal to principal stresses	$P_f = \sigma_n + \dfrac{(C_e - \tau)}{\mu_s}$	—
Stylolitic solution planes	envelope $\perp r\,\sigma_1$	?	fine-grained rock matrix

grain-scale tensile microcracks which, as a consequence of stress heterogeneities arising from grain impingement, form over a range of orientations but statistically show a preferential alignment perpendicular to σ_3; (ii) *macroscopic extension fractures* forming perpendicular to σ_3 by hydraulic extension fracturing (Secor 1965); (iii) *macroscopic shear fractures (faults)* developing in planes containing the σ_2 direction and lying at angles, typically $\pm 20° < \theta_s < \pm 30°$, to σ_1 (Anderson 1951); (iv) *hybrid extensional-shear fractures* developing in planes which also contain the σ_2 direction but lie at lower angles ($\theta_{es} < \theta_s$) to σ_1 (Hancock 1985) and, (v) *stylolitic solution planes* developing as anticracks (Fletcher & Pollard 1981) in planes perpendicular to σ_1 (Fig. 5a). Existing planar contacts, with or without inherent cohesive strength, may also be reactivated.

The type of brittle failure that occurs as a consequence of pressurised fluid infiltration at a particular point in stressed heterogeneous crust therefore depends largely on the balance between the differential stress and local tensile rock strength, both of which may vary considerably. As an individual structure forms, the local stress field becomes further perturbed through interactions with existing mesh components (Segall & Pollard 1980), adding to stress heterogeneity within the evolving fault–fracture system. A complex mesh of different brittle structures may then develop in response to the heterogeneity of material properties, stress, and fluid pressure within the rock-mass, with the orientation of any one type of mesh component showing considerable variance.

Formation of different structural elements within a mesh may affect rock-mass permeability in a variety of ways. For example, while faulting in low-porosity rock will generally increase fracture permeability as a consequence of cataclastic brecciation, faulting in initially high-porosity sedimentary rock may lead to the formation of reduced permeability 'deformation bands' through porosity collapse and comminution (Aydin & Johnson 1978). Another important point is that much of the structural permeability developed in fault–fracture meshes is likely to be transitory, as microcracks, fractures and faults may all become infilled with low-permeability hydrothermal precipitates, alteration products, and/or clay-rich gouge. Permeability enhancement through faulting and fracturing in hydrothermal systems competes with permeability reduction as a consequence of fluid flow and precipitation (Henley 1984), so that deformation within fault–fracture meshes, either continual or intermittent, is probably necessary for them to remain effective as high-permeability structural conduits (Sibson 1994).

Factors affecting mesh development

General factors favouring mesh formation include material heterogeneity within the rock mass (so that the stress state and/or the tensile strength vary from place to place) and low effective stress conditions. Layered rock sequences are particularly susceptible to mesh development, especially in extensional tectonic regimes, because

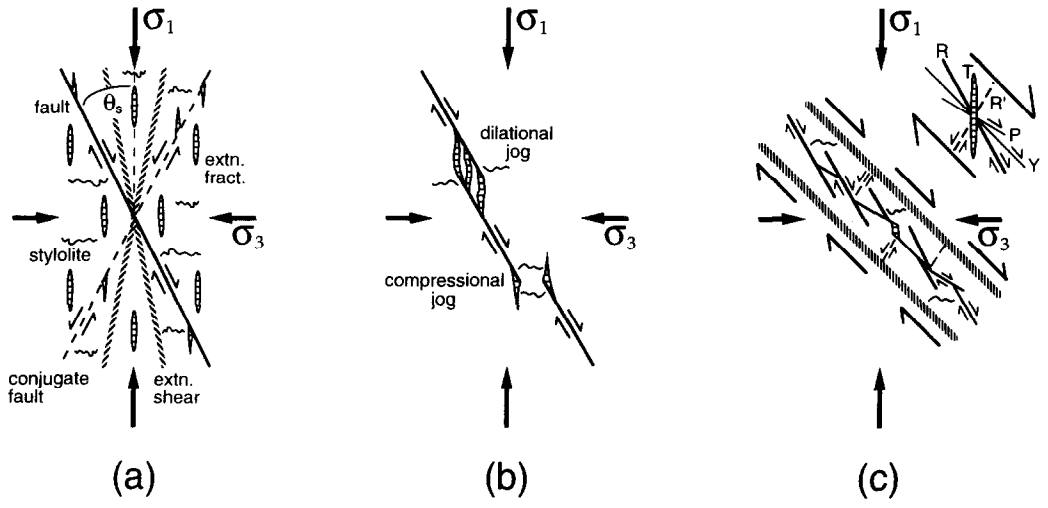

Fig. 5. (a) Stress-controlled mesh components; (b) segmented fault with linking compressional and dilational jogs (after Segall & Pollard 1980); (c) throughgoing fault developed from a Riedel shear mesh (after Tchalenko 1970). Note that the common intersection of mesh components is the σ_2 direction.

the brittle failure mode is then dictated by the tensile strength of alternating rock layers (Sibson 1994, Gross 1995, Gross & Engelder 1995). In such cases, layer thickness may impose a scale on the mesh structure that develops. Mesh structures incorporating extensional-shear and/or extension fractures require the condition $P_f \sim \sigma_3$ to be met, at least locally, and are unlikely to develop where effective stress is high.

In more homogeneous rock-masses, an additional factor promoting mesh formation within extensional and strike-slip regimes is the limited vertical extent of individual hydraulic extension fractures. Secor & Pollard (1975) pointed out that while the fluid pressure at the top of a vertical fluid-filled crack must exceed the least compressive stress to meet the tensile failure criterion (Table 1), the hydrostatic fluid pressure gradient within the crack will, in general, be less than the vertical gradient of σ_3 in the wallrock. Such cracks can, therefore, only remain open over the limited depth range where $P_f > \sigma_3$. They suggested an upper limit of perhaps 100 m or so for individual vertical hydrofractures in crystalline rock. Outside this restricted interval, fluid pressure conditions favour shear failure, with the possibility of an interlinked fault–fracture mesh developing as overpressured fluids migrate along a hydraulic gradient.

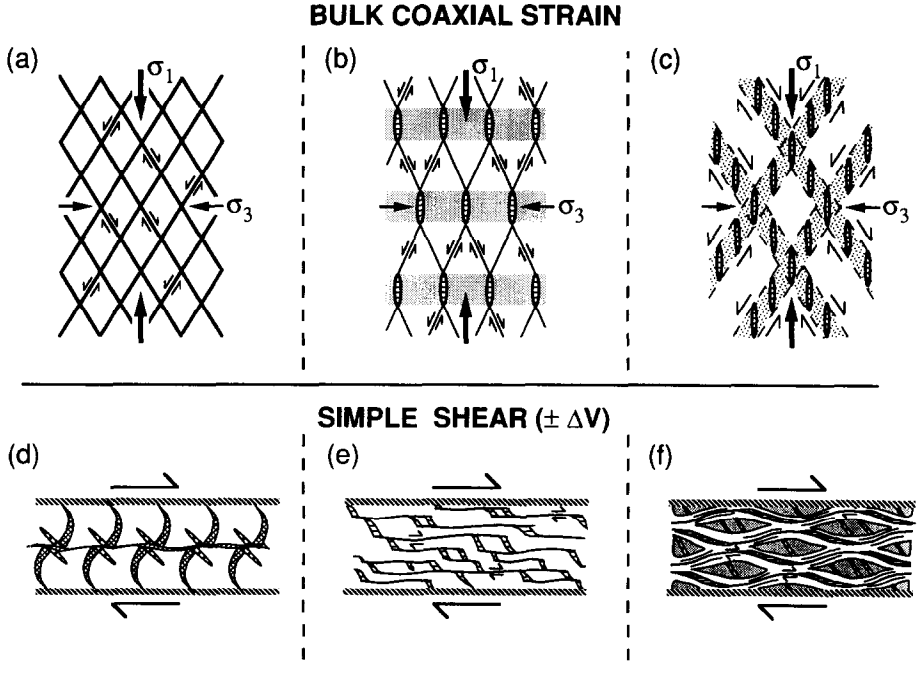

Fig. 6. Varieties of fault–fracture mesh: *Bulk Coaxial Strain* (a) conjugate Coulomb shears; (b) Hill-type mesh in alternating competent and incompetent strata; (c) conjugate tension gash shear zone mesh; *Simple Shear* ($\pm$ ΔV); (d) sheared-out tension gash shear zone; (e) interlinked shears and dilational jogs; (f) 'dead-fish' shear zone with anastomosing slickenfibre surfaces interlinked by extension fractures in competent phacoids. Common intersection of mesh components is again the σ_2 direction.

VARIETIES OF FAULT–FRACTURE MESH

Characteristic orientations of the basic structural elements with respect to the local stress field are given in Fig. 5(a), along with simple combinations of the different structural elements that are likely to develop in individual brittle to semi-brittle shear zones as a consequence of *en echelon* segmentation (Fig. 5b) (Segall & Pollard 1980), or through the amalgamation of Riedel shear arrays (Fig. 5c) (Tchalenko 1970). Different structural elements may combine in various combinations to build more extensive fault–fracture meshes (Fig. 6). Not all components need be present in every case.

Fault–fracture meshes accommodating bulk coaxial strain are most likely to develop when the symmetry of the dominant anisotropy in the rock mass (e.g. bedding) and the prevailing stress field coincide. These structures form a continuum with a varying content of extension fractures, ranging from arrays of conjugate Coulomb shears, through Hill-type fault–fracture meshes, to conjugate tension gash shear zones (Figs. 6a–c and 7a–d). Hill-type meshes are commonly well developed where beds of strong competence contrast are interlayered, as in the oil-rich Monterey Formation of coastal California (comprising interbedded dolostones, limestones, siliceous shales, and mudstones) which is notable for the manner in which the mode of brittle failure varies with lithology (Gross 1995, Gross & Engelder 1995) (Figs. 7a & b).

In situations approximating bulk simple shear with a large component of rotational strain, the resulting mesh structure is likely to be less regular. Various combinations of tension gash shear zones formed by hydraulic fracturing interlinked with discrete shear surfaces may develop. Figure 6(e)–(f) are schematic representations of different styles of shearing in the Chrystall's Beach Complex, interpreted as part of a Mesozoic accretionary melange by Nelson (1982). In thicker pelitic units within the complex, quartz and calcite slickenfibre sliding surfaces dispersed on scales of centimetres to metres throughout the complex are interlinked through dilational jogs to form a shear zone mesh (Figs. 6e and 7e). Elsewhere, dismembered lenses of comparatively competent sandstone in a highly strained pelitic matrix are cut by arrays of extension veins and bounded by anastomosing slickenfibre surfaces (Figs. 6f and 7f).

Orientation of mesh structures is dictated by the vertical stress associated with different tectonic regimes (Anderson 1951). In extensional regimes with $\sigma_v = \sigma_1$, mesh components may include steeply-dipping normal faults in conjugate sets interlinked with subvertical extension fractures and subhorizontal stylolites, while in a compressional regime with $\sigma_v = \sigma_3$, a mesh structure may involve conjugate gently-dipping thrust faults interlinked with subhorizontal extension fractures and subvertical stylolites. In a strike-slip regime with $\sigma_v = \sigma_2$, a mesh may comprise subvertical extension fractures, stylolites and conjugate strike-slip faults. Petit & Mattauer (1995) have recently described just such a strike-slip mesh structure, with a mesh dimension of ~ 10 m perhaps dictated by an inherited semi-brittle fabric, in Jurassic limestone strata affected by Pyrenean deformation in the Languedoc region of southern France.

Note that because of crustal heterogeneity, the tendency for individual shears to terminate laterally in *en echelon* tension crack arrays as well as at their tips (McGrath & Davison 1995), and for complex interactions to develop between mesh components, the 3-D mesh structure will generally be a great deal more complicated than the 2-D 'plane strain' diagrams in Figs. 5 and 6 suggest. Additional complexities may arise from the formation of orthorhombic fault systems to accommodate bulk strains in three dimensions (Reches 1983). Moreover, with increasing displacement some mesh structures may evolve into throughgoing planar faults that are favourably oriented in the prevailing stress field and no longer require the same degree of overpressuring for reactivation. Mesh development in regions of high fluid pressure may thus be a precursor to the development of major new fault structures.

σ_2 directional permeability in fault–fracture meshes

Microscopic and macroscopic extension fracturing enhances permeability in the σ_1/σ_2 plane, the effect becoming more pronounced as the fluid pressure approaches σ_3, and the effective least compressive stress, $\sigma_3' = (\sigma_3 - P_f)$ tends to zero. Unhealed fault surfaces forming in low-porosity rock, through their intrinsic roughness, also provide permeable channelways. The common intersection of faults and extension fractures thus enhances rock-mass permeability by adding a tubular component in the σ_2 direction (see Figs. 5 and 6), perpendicular to fault slip vectors (cf. Snow 1969). Directional permeability in the σ_2 direction is also likely to develop when a conjugate fault mesh forms in rock with high initial porosity and permeability; reduced permeability along the faults through comminution and porosity collapse (Aydin & Johnson 1978) then bounds 'tubes' of high permeability in the intervening rock-mass (Fig. 6a). Stylolitic solution seams with their residue of impermeable clay minerals also represent tabular zones of reduced porosity (Groshong 1988, Carrio-Schaffhauser *et al.* 1990) that restrict flow perpendicular to the

Fig. 7. Photographs of mesh structures: (a, b) varieties of Hill-type extensional fault–fracture meshes (conjugate normal faults, subvertical extension fractures and extensional shears), with infillings of calcite and bitumen from the Miocene Monterey Formation of interbedded dolostones, limestones, siliceous shales, and mudstones, Arroyo Burro Beach, Santa Barbara; (c) conjugate quartz tension-gash shear zone mesh with spaced solution cleavage (dark striping) developed in a bed of Old Red Sandstone, Marloes Sands, SW Wales; (d) compressional fault–fracture mesh with conjugate thrust faults and associated hydraulic extension fractures infilled with quartz–prehnite and laumontite–calcite assemblages in steeply-dipping interbedded greywacke sandstones and argillites, east abutment, Benmore Dam, Waitaki Valley, New Zealand; (e, f) quartz and calcite slickenfibre sliding surfaces interlinked with extension fractures and dilational jogs in sheared sandstone–shale melange, Chrystalls Beach accretionary complex, SE Otago coast, New Zealand.

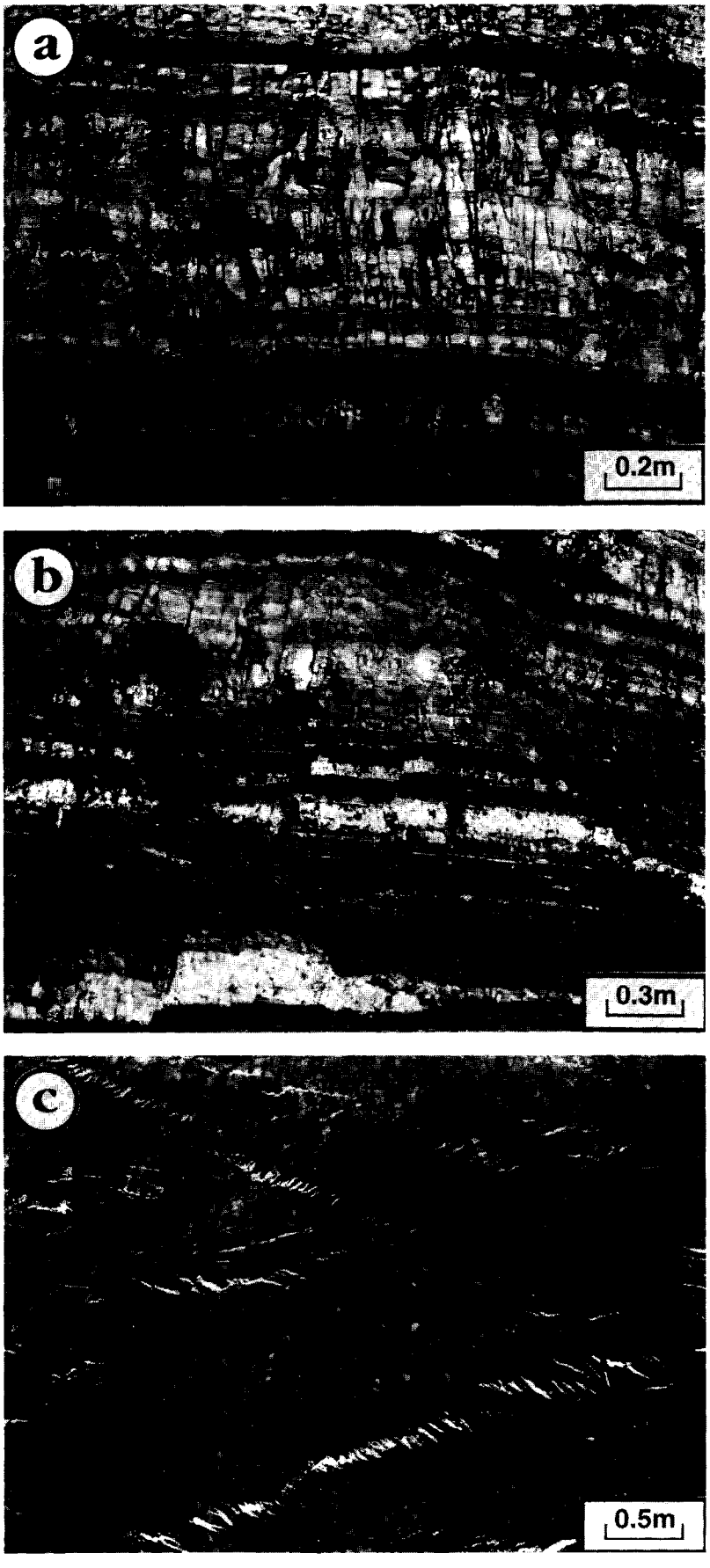

Fig. 7. (a)–(c).

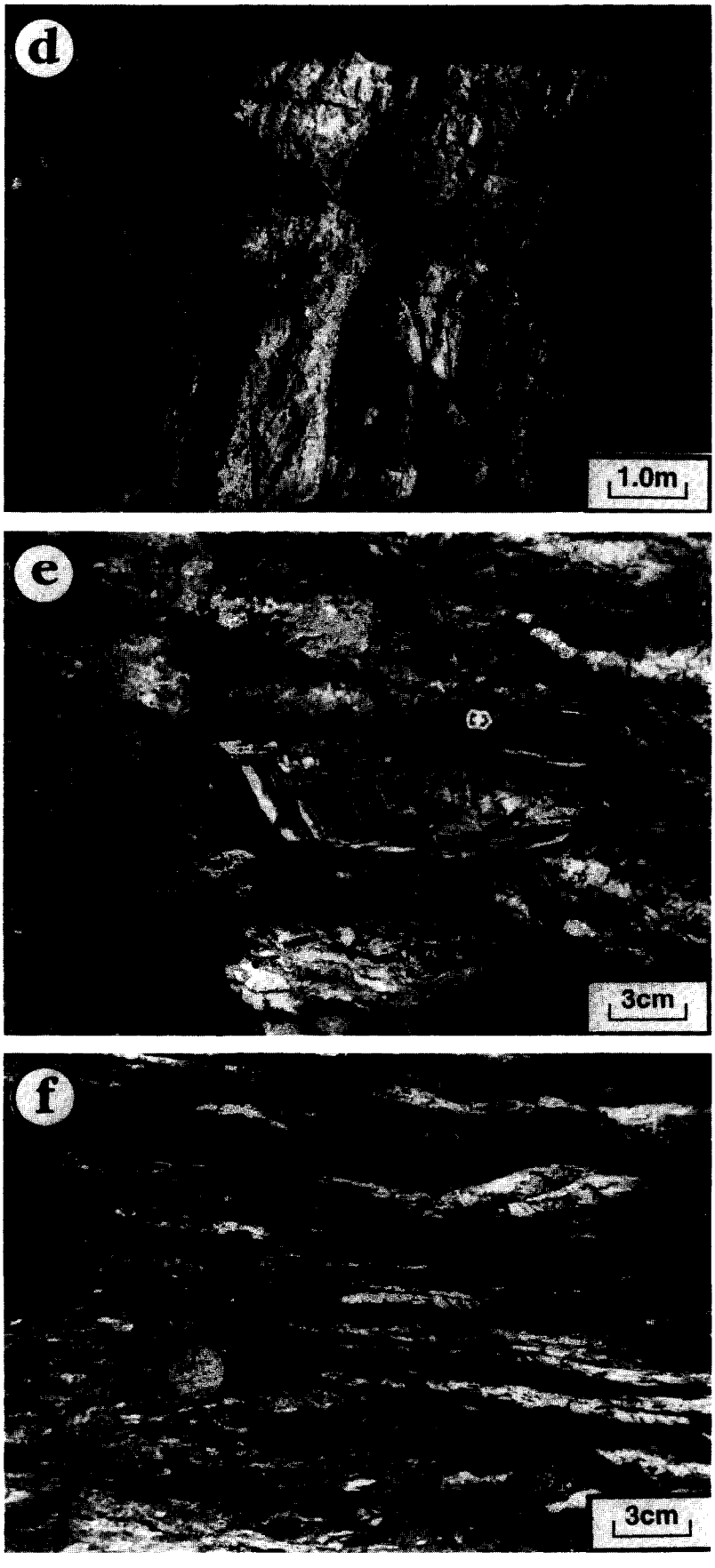

Fig. 7. (d)–(f).

σ_2/σ_3 plane in which they form (Fletcher & Pollard 1981). Overall, the combined effect of all these structural elements is to impart directional permeability along the average σ_2 direction within the rock mass, though the extent of the effect will depend on the 3-D interconnectedness of the different structural elements.

FLUID PRESSURE CONTROLS ON MESH ACTIVATION

The level of fluid pressure at depth, z, in the crust can be expressed in terms of the pore-fluid factor, $\lambda_v = (P_f/\sigma_v) = (P_f/\rho g z)$, where ρ is the average rock density and g is the gravitational acceleration. In crust with fluid-saturated pore and/or fracture space interconnected to the Earth's surface, hydrostatic conditions prevail with $\lambda_v = \rho_f/\rho \approx 0.4$. Actively deforming portions of the crust are, however, commonly overpressured at depth with $\lambda_v \rightarrow 1$ ($\sim$lithostatic fluid pressure conditions) in some circumstances (Fyfe *et al.* 1978). Overpressuring may arise from burial compaction in thick sedimentary sequences, metamorphic dewatering in the middle to deep crust, thermal overpressuring from magmatic intrusion, and mantle degassing. All may contribute to suprahydrostatic vertical fluid pressure gradients, but strong lateral hydraulic gradients may also develop, particularly adjacent to magmatic intrusions. What, then, are the fluid pressure conditions for mesh activation at different depths in different tectonic regimes?

To function as high permeability conduits promoting flow of large fluid volumes, mesh structures must incorporate a significant proportion of gaping extension fractures and extensional shears. Formation of such structures in relatively competent material requires $P_f > \sigma_3$ and $(\sigma_1 - \sigma_3) < 4T$ locally (Table 1), but the stress field throughout the mesh will be very inhomogeneous. However, on a gross scale, a Hill-type mesh can be regarded kinematically as equivalent to a single extension fracture; on these grounds, the condition, $P_f \approx \sigma_3$ (where σ_3 is the average least stress at a particular depth) is adopted here as an approximate criterion for mesh activation and large volume fluid flow. Because hydraulic extension fracturing is integral to the formation of higher permeability meshes and $T < 10$ MPa for most competent rocks (Etheridge 1983), the upper bound to differential stress during mesh propagation is taken as 40 MPa.

Adapting the procedure developed by Secor (1965), the fluid pressure conditions for mesh activation at different depths in the crust are expressed on a plot of the pore-fluid factor, λ_v, versus depth, z, for different stress regimes assuming a maximum differential stress of 40 MPa (Fig. 8). Note that for lesser values of rock tensile strength and permissible differential stress, the λ_v values needed for hydrofracturing at a particular depth will be higher. From the λ_v/z plot it is apparent that whereas mesh activation in a compressional thrust-fault regime ($\sigma_v = \sigma_3$) requires lithostatic fluid pressures ($\lambda_v \sim 1$) at all depths, activation of fault–fracture meshes with large-

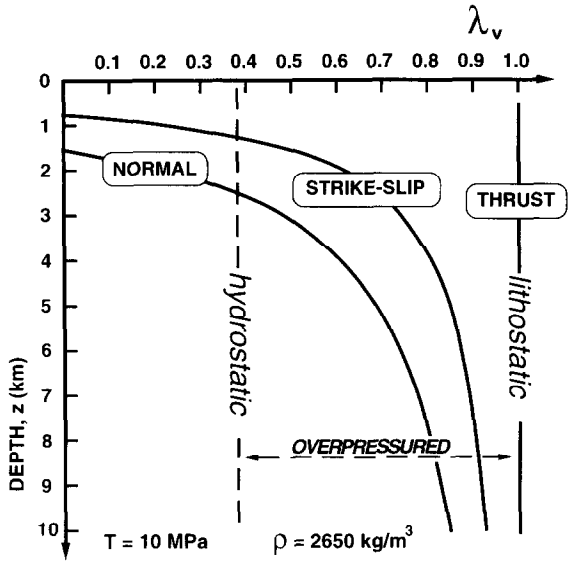

Fig. 8. Fluid pressure conditions for activation of fault–fracture meshes in compressional thrust-fault, extensional normal-fault, and strike-slip regimes expressed on a plot of pore-fluid factor, λ_v, versus depth for the limiting condition $(\sigma_1 - \sigma_3) < 4T = 40$ MPa.

volume fluid flow can occur under hydrostatic or lower fluid pressure levels ($\lambda_v \leq 0.4$) at shallow depths in an extensional normal-fault regime ($\sigma_v = \sigma_1$). In strike-slip regimes ($\sigma_v = \sigma_2$), the fluid pressure condition for mesh activation can lie anywhere between the extensional situation when $\sigma_v = \sigma_2 \sim \sigma_1$ in a transtensional setting, and the compressional situation when $\sigma_v = \sigma_2 \sim \sigma_3$ under transpression. The case illustrated is for the intermediate situation where $\sigma_v = \sigma_2 = \frac{1}{2}(\sigma_1 + \sigma_3)$. At greater depths in extensional–transtensional settings, fluid overpressures ($0.4 < \lambda_v < 1.0$) are needed to activate mesh structures as high permeability conduits.

The extent and rate of mesh development and propagation will be strongly affected by fluid supply, the maintenance of an appropriate hydraulic gradient, and the permeability characteristics of the rock mass. It seems probable that active fault–fracture meshes can be regarded as buoyant, overpressured 'fluid domains' of the kind envisaged by Gold & Soter (1985). They pointed out that many of the time-dependent and migratory characteristics of earthquake sequences are explicable in terms of transitory linkages ('burping') within a stack of overpressured fluid domains; this concept seems likely to be especially applicable to swarm activity.

TECTONIC ENVIRONMENTS FOR MESH FORMATION

The predominant association of earthquake swarms with areas of active extensional and transtensional tectonics suggests that fault–fracture meshes are widely developed in such settings where they likely play an important role in the formation of hydrothermal mineral deposits. Established hydrothermal plumes in such areas are close to hydrostatically pressured, at least in the near-surface (Henley 1984), and may either be localised by

existing fault–fracture mesh conduits or have contributed to their generation. Mesh activation in extensional regimes is strongly favoured at shallow depths (generally <1 km) in the vicinity of the hydrostatic boiling horizon (Fig. 8), and must inevitably contribute to fluid focusing and the generation of epithermal mineralisation.

In this regard, it is interesting to note the intense shallow ($z < 5$ km) microseismicity from distributed normal faulting, somewhat akin to swarm seismicity, that extends around areas of steam extraction and high flow rate in the Geysers geothermal field of northern California (Oppenheimer 1986). Towards the base of the field there is evidence for a transition from a hydrostatic to a strongly overpressured hydrothermal regime (Fournier 1991). It is tempting to believe that the microseismic activity arises from fluid migration through a fault–fracture mesh developed across this transition region, representing a form of distributed fault-valve action along a suprahydrostatic fluid pressure gradient.

Detailed seismicity studies within the San Andreas fault system have revealed other zones of clustered microearthquake activity that, akin to swarms, may define zones of overpressured fluid migration (Hill *et al.* 1990). Along creeping segments of the fault system, the full depth of the seismogenic zone down to 10–15 km is intensely microseismically active. This globally anomalous slip behaviour has previously been attributed (Irwin & Barnes 1975) to the trapping of overpressured fluids within the strike-slip faults beneath a capping serpentinite seal associated with the Coast Range Thrust. The mechanical inference developed here is that the coupling of microearthquake clusters to aseismic slip in such regions likely involves simple shear across a tabular fault–fracture mesh, developed in response to a near-lithostatic fluid pressure profile, that extends from the near-surface to the base of the seismogenic zone.

Elsewhere, along some of the locked portions of the San Andreas system, the base of the seismogenic zone is defined by a band of microearthquake activity with a vertical extent of a few kilometres. The interpretation here is that the structural level at the base of the seismogenic zone, defining the onset of greenschist facies metamorphic conditions, is associated with upwards migration of fluids, accompanied by mesh development, across the transition from a near-lithostatic to a sub-lithostatic fluid pressure environment. Interestingly, this is the structural level in the crust where mesothermal gold–quartz lodes (occupying fault–fracture meshes <2 km in vertical extent) most commonly develop by fault-valve action across steep hydraulic gradients (Sibson *et al.* 1988). While the extreme fault-valve action that gives rise to such major vein systems is generally restricted to steep reverse faults that are severely misoriented for reactivation, less intense episodic fluid migration at this crustal level seems likely to be a feature of most transcrustal fault zones (Sibson 1994).

Swarm activity is comparatively rare in compressional settings but is known from the fold–thrust belt in the Santa Barbara Channel which, at least locally, is known to be overpressured to near-lithostatic values (Yeats 1983). A recent swarm in 1984 occurred at depths of 7–15 km directly beneath one of the major oil-fields (Shaw & Suppe 1994), apparently along a steep reverse fault; the most favourable structural setting for extreme valving action (Sibson 1990).

Mesh structures as fluid conduits in different tectonic settings

The direction of fluid flow through a rock mass is governed by the maximum hydraulic gradient (not necessarily vertical), existing permeability anisotropy (e.g. bedding, foliation), and superimposed structural permeability. Particular combinations of these parameters may lead to the localised high-volume flows needed to develop hydrothermal mineral deposits. Favoured localities for mesh development include short-lived irregularities along large-displacement fault zones such as dilational jogs, lateral ramps, transfer faults, and other forms of link structure. In the case of strike-slip faulting, obvious examples of enhanced permeability in fault–fracture meshes parallel to vertical σ_2 include the Matsushiro swarm, and the localisation of both magmatism and associated upwelling hydrothermal plumes in major dilational jogs along the San Andreas fault in the Salton Sea area of California (Weaver & Hill 1979, Sibson 1987). Different combinations of hydraulic gradient, intrinsic permeability anisotropy and structural permeability may, however, lead to more complex 3-D flow paths as in the situations outlined in Fig. 9.

Figure 9(a) illustrates a situation where, despite a vertical gradient in hydraulic potential, the presence of a gently raking dilational jog on a normal fault localises and deflects flow laterally along the jog structure. Such features might account for the localisation of hot spring activity at particular sites along normal faults, as occurs within the Taupo Volcanic Zone in New Zealand. In Fig. 9(b), development of a Hill (1977) fault–fracture mesh in a sequence of gently dipping interbedded competent and incompetent strata promotes flow up-dip (cf. Fig. 7a). Dilational jogs associated with reverse slip on bedding-parallel faults during progressive fold tightening and amplification (Fig. 9c) induce along-strike migration into hinge-line culminations, as demonstrated for the Wattle Gully Au–quartz vein system in the Lachlan fold belt of Victoria, Australia (Cox *et al.* 1991); this mechanism may also assist the syntectonic migration of hydrocarbons into antiformal reservoirs. The effect of a strong lateral hydraulic gradient adjacent to a high-level pluton, coupled with the high σ_2 permeability of an extensional fault–fracture mesh, leads to strongly focused lateral flow (Fig. 9d). This situation resembles the structures hosting tin mineralisation around the cupolas of the Cornubian batholith in SW England (Moore 1975), and may also have relevance to the localisation of some geothermal fields in the Taupo Volcanic Zone near the intersections of the active belt of normal faults with major ring structures defining buried calderas (Cole 1990).

These examples, all involving predominantly dip-slip faulting, illustrate how migration paths for escaping

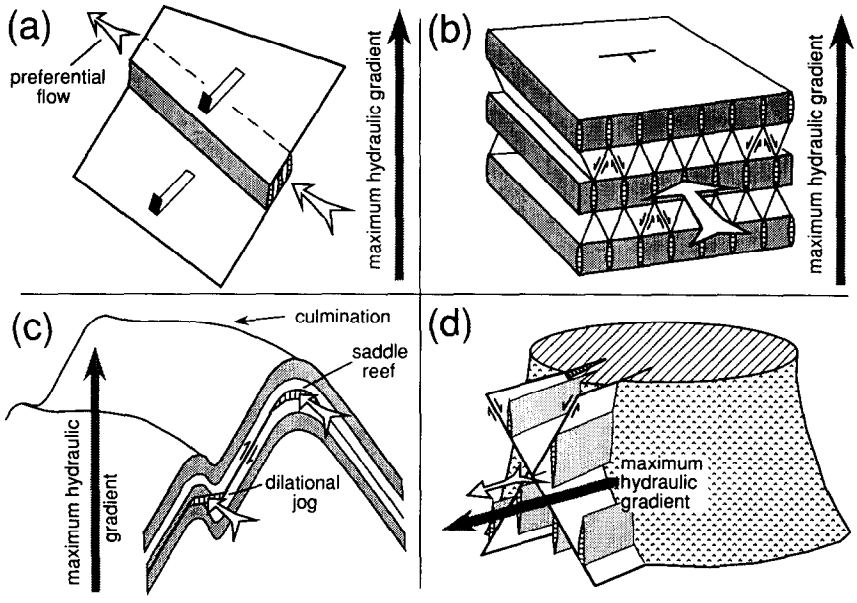

Fig. 9. Mesh structures in different tectonic settings illustrating the effects of σ_2 permeability enhancement: (a) gently raking dilational jog on normal fault; (b) Hill-type fault–fracture mesh in gently dipping interbedded competent and incompetent strata; (c) dilational jogs and saddle reefs associated with bedding plane reverse-slip, promoting along axis flow into fold culminations; (d) extensional normal-fault mesh abutting plutonic contact with intense lateral hydraulic gradient.

overpressured fluids may be deflected from the vertical by directional stress-controlled permeability. This could help to account for the rapid lateral, as well as vertical, migration of swarm activity that is sometimes observed (Grindley & Hull 1986).

DISCUSSION

This paper has addressed two principal themes. The first is the self-generation of structural permeability in different stress regimes by migrating fluids and its importance in promoting the large-volume fluid flow needed to form hydrothermal ore deposits. Stress-controlled structural permeability may also play an important role in hydrocarbon migration (Du Rouchet 1981). The second theme concerns the extent to which microearthquake swarms or clusters may be used to define active fault–fracture meshes in different tectonic settings. At other than very shallow depths in extensional–transtensional settings, such swarm activity probably represents migration of overpressured fluids along suprahydrostatic fluid pressure gradients (cf. Gold & Soter 1985). This is of particular interest given recent recognition that intermittent breaching of overpressured fluid compartments in sedimentary basins leads to episodes of fluid migration (Hunt 1990, Powley 1990), and the expectation of similar behaviour in and around crustal fault zones (Sibson 1981, 1990, Byerlee 1993).

Persistent swarm activity at shallow depths (<4 km deep, say) is an attractive target for scientific drilling and other forms of geophysical investigation to test the hypothesis that swarms are associated with the migration of overpressured fluids. Penetration of swarms by drilling would allow direct measurement of fluid pressure levels, while sustained measurements might allow correlation of seismic activity with local changes in fluid pressure. Mesh propagation could be expected to induce localized ΔP_f fluctuations of the order of the rock's tensile strength (1–10 MPa). Correlations between swarm activity, surface deformation, hydrological fluctuations and groundwater chemistry, as at Matsushiro, have the potential to yield information on mesh dimensions and rates of fluid flow.

Important conclusions of this paper are that the distribution of fluid overpressures in the crust exerts a strong influence on the style of faulting and patterns of mineralisation, that varying seismic style in different tectonic settings may be a key to understanding different types of mineralising environment, and that structural permeability analysis has the potential to become an important part of both mineral and hydrocarbon exploration.

Acknowledgements—Research leading to this paper forms part of a study funded from the Public Good Science Fund by Grant UO-0312 from the New Zealand Foundation for Research, Science, and Technology. Many of the ideas developed here arose from conversations over the years with Neville Price and Dave Hill. I thank John Scott, Joe Cartwright and Mike Blanpied for helpful criticism.

REFERENCES

Anderson, E. M. 1951. *The Dynamics of Faulting and Dyke Formation with Application to Britain* (2nd edn). Oliver and Boyd, Edinburgh.

Aydin, A. & Johnson, A. M. 1978. Development of faults as zones of deformation bands and as slip surfaces in sandstones. *Pure & Appl. Geophys.* **116**, 932–942.

Brace, W. F. 1960. An extension of the Griffith theory of fracture to rocks. *J. geophys. Res.* **65**, 3477–3480.

Byerlee, J. D. 1993. Model for episodic flow of high-pressure water in fault zones before earthquakes. *Geology* **21**, 303–306.

Carrio-Schaffhauser, E., Raynaud, S., Latiere, H. J. & Mazerolle, F. 1990. Propagation and localisation of stylolites in limestones. In:

Deformation Mechanisms, Rheology and Tectonics (edited by Knipe, R. J. & Rutter E. H.). *Spec. Publs geol. Soc. Lond.* **54**, 193–199.
Cole, J. W. 1990. Structural control and origin of volcanism in the Taupo Volcanic Zone, New Zealand. *Bull. Volcanol.* **52**, 445–459.
Cox, S. F., Wall, V. J., Etheridge, M. A. & Potter, T. F. 1991. Deformational and metamorphic processes in the formation of mesothermal vein-hosted gold deposits—examples from the Lachlan Fold Belt in central Victoria, Australia. *Ore Geol. Rev.* **6**, 391–423.
Du Rouchet, J. 1981. Stress fields, a key to oil migration. *Bull. Am. Ass. Petrol. Geol.* **65**, 74–85.
Etheridge, M. A. 1983. Differential stress magnitudes during regional deformation and metamorphism: upper bound imposed by tensile fracturing. *Geology* **11**, 231–234.
Fletcher, R. C. & Pollard, D. D. 1981. Anticrack model for pressure solution surfaces. *Geology* **9**, 419–424.
Fournier, R. O. 1991. The transition from hydrostatic to greater than hydrostatic fluid pressures in presently active hydrothermal systems in crystalline rock. *Geophys. Res. Lett.* **18**, 955–958.
Fyfe, W. S., Price, N. J. & Thompson, A. B. 1978. *Fluids in the Earth's Crust*. Elsevier, Amsterdam.
Gold, T. & Soter, S. 1985. Fluid ascent through the solid lithosphere and its relation to earthquakes. *Pure & Appl. Geophys.* **122**, 492–530.
Grindley, G. W. & Hull, A. G. 1986. Historical Taupo earthquakes and earth deformation. *Roy. Soc. N. Z. Bull.* **24**, 173–185.
Groshong, R. H. 1988. Low temperature deformation mechanisms and their interpretation. *Bull. geol. Soc. Am.* **100**, 1329–1360.
Gross, M. R. 1995. Fracture partitioning: failure mode as a function of lithology in the Monterey Formation of coastal California. *Bull. geol. Soc. Am.* **107**, 779–792.
Gross, M. R. & Engelder, T. 1995. Strain accommodated by brittle failure in adjacent units of the Monterey Formation, U.S.A.: scale effects and evidence for uniform displacement boundary conditions. *J. Struct. Geol* **17**, 1303–1318.
Hagiwara, T. & Iwata, T. 1968. Summary of the seismographic observation of Matsushiro swarm earthquakes. *Bull. Earthq. Res. Inst. Tokyo Univ.* **46**, 485–515.
Hancock, P. L. 1985. Brittle microtectonics: principles and practice. *J. Struct. Geol.* **7**, 437–457.
Healy, J. H., Rubey, W. W., Griggs, D. T. & Raleigh, C. B. 1968. The Denver earthquakes. *Science* **161**, 1301–1310.
Henley, R. W. 1984. The geothermal framework of epithermal deposits. In: *Geology and Geochemistry of Epthermal Systems* (edited by Berger, B. R. & Bethke, P. M.). *Soc. Econ. Geol. Rev. Econ. Geol.* **2**, 1–24.
Hill, D. P. 1977. A model for earthquake swarms. *J. geophys. Res.* **82**, 347–352.
Hill, D. P., Eaton, J. P. & Jones, L. 1990. Seismicity, 1980–86. In: *The San Andreas Fault System* (edited by Wallace, R. E.). *U.S. Geol. Surv. Prof. Paper* **1515**, 114–151.
Hubbert, M. K. & Rubey, W. W. 1959. Role of fluid pressure in mechanics of overthrust faulting. *Bull. geol. Soc. Am.* **70**, 115–166.
Hunt, J. M. 1990. Generation and migration of petroleum from abnormally pressured fluid compartments. *Bull. Am. Ass. Petrol. Geol.* **74**, 1–12.
Ichikawa, M. 1969. Matsushiro earthquake swarm. *Geophys. Mag.* **34**, 307–331.
Irwin, W. P. & Barnes, I. 1975. Effects of geologic structure and fluids on the seismic behaviour of the San Andreas fault system in central and northern California. *Geology* **3**, 713–716.
Kisslinger, C. 1975. Processes during the Matsushiro earthquake swarm as revealed by levelling, gravity, and spring-flow observations. *Geology* **3**, 57–62.
Lee, W. H. K., Eaton, M. S. & Brabb, E. E. 1971. The earthquake sequence near Danville, California, 1970. *Bull. seism. Soc. Am.* **61**, 1771–1794.
McGrath, A. G. & Davison, I. 1995. Damage zone geometry around fault tips. *J. Struct. Geol.* **17**, 1011–1024.
McKinstry, H. E. 1948. *Mining Geology*. Prentice-Hall, Englewood Cliffs, New Jersey.
Mogi, K. 1963. Some discussions on aftershocks, foreshocks, and earthquake swarms—the fracture of a semi-infinite body caused by an inner stress origin and its relation to the earthquake phenomenon, 3. *Bull. Earthq. Res. Inst. Tokyo Univ.* **41**, 615–658.
Mogi, K. 1988. The mechanism of the Matsushiro earthquake swarm in central Japan and its relation to the 1964 Niigata earthquake. *Tectonophysics* **159**, 109–119.
Moore, J. M. 1975. A mechanical interpretation of the vein and dyke systems of the SW England orefield. *Miner. Deposita* **10**, 374–388.
Morimoto, R., Nakamura, K., Tsuneishi, Y., Ossaka, J. & Tsunoda, N. 1967. Landslides in the epicentral area of the Matsushiro earthquake swarm—their relation to the earthquake fault. *Bull. Earthq. Res. Inst. Tokyo Univ.* **45**, 241–263.
Nakamura, K. 1971. A hypothesis on the mechanism of the Matsushiro earthquake swarm. *Kagaku-Asahi* **10**, 127–133.
Nelson, K. D. 1982. A suggestion for the origin of mesoscopic fabric in accretionary melange, based on features observed in the Chrystalls Beach Complex, South Island, New Zealand. *Bull. geol. Soc. Am.* **93**, 625–634.
Newhouse, W. H. 1942. *Ore Deposits as Related to Structural Features*. Princeton University Press, Princeton, New Jersey.
Nur, A. 1974. Matsushiro, Japan, earthquake swarm: confirmation of the dilatancy–fluid diffusion model. *Geology* **2**, 217–221.
Oppenheimer, D. H. 1986. Extensional tectonics at The Geysers geothermal area, California. *J. geophys. Res.* **91**, 11,463–11,476.
Petit, J.-P. & Mattauer, M. 1995. Paleostress superimposition deduced from mesoscale structures in limestone: the Matelles exposure, Languedoc, France. *J. Struct. Geol.* **17**, 245–256.
Powley, D. E. 1990. Pressures and hydrogeology in petroleum basins. *Earth Sci. Rev.* **29**, 215–226.
Raleigh, C. B., Healy, J. H. & Bredehoeft, J. D. 1976. An experiment in earthquake control at Rangeley, Colorado. *Science* **191**, 1230–1236.
Reches, Z. 1983. Faulting of rocks in three-dimensional strain fields II. Theoretical analysis. *Tectonophysics* **95**, 133–156.
Scholz, C. H. 1968. The frequency–magnitude relation of microfracturing in rock and its relation to earthquakes. *Bull. seism. Soc. Am.* **58**, 399–415.
Secor, D. T. 1965. Role of fluid pressure in jointing. *Am. J. Sci.* **263**, 633–646.
Secor, D. T. & Pollard, D. D. 1975. On the stability of open hydraulic fractures in the Earth's crust. *Geophys. Res. Lett.* **2**, 510–513.
Segall, P. & Pollard, D. D. 1980. Mechanics of discontinuous faults. *J. geophys. Res.* **85**, 4337–4350.
Shaw, J. H. & Suppe, J. 1994. Active faulting and growth folding in the eastern Santa Barbara Channel, California. *Bull. geol. Soc. Am.* **106**, 607–626.
Sibson, R. H. 1981. Fluid flow accompanying faulting: field evidence and models. In: *Earthquake Prediction: an International Review* (edited by Simpson, D. W. & Williams, P. G.). *Am. Geophys. Union, Maurice Ewing Series* **4**, 593–603.
Sibson, R. H. 1987. Earthquake rupturing as a hydrothermal mineralising agent. *Geology* **15**, 701–704.
Sibson, R. H. 1989. Earthquake faulting as a structural process. *J. Struct. Geol.* **11**, 1–14.
Sibson, R. H. 1990. Conditions for fault-valve behaviour. In: *Deformation Mechanisms, Rheology and Tectonics* (edited by Knipe, R. J. & Rutter, E. H.). *Spec. Publ. geol. Soc. Lond.* **54**, 15–28.
Sibson, R. H. 1994. Crustal stress, faulting, and fluid flow. In: *Geofluids: Origin, Migration and Evolution of Fluids in Sedimentary Basins* (edited by Parnell, J.). *Spec. Publs geol. Soc. Lond.* **78**, 69–84.
Sibson, R. H., Robert, F. & Poulsen, K. H. 1988. High-angle reverse faults, fluid-pressure cycling, and mesothermal gold–quartz deposits. *Geology* **16**, 551–555.
Snow, D. T. 1969. Anisotropic permeability of fractured media. *Water Resourc. Res.* **5**, 1273–1289.
Stuart, W. D. & Johnston, M. J. S. 1975. Intrusive origin of the Matsushiro earthquake swarm. *Geology* **3**, 63–67.
Sykes, L. R. 1970. Earthquake swarms and sea-floor spreading. *J. geophys. Res.* **75**, 6598–6611.
Tchalenko, J. S. 1970. Similarities between shear zones of different magnitudes. *Bull. geol. Soc. Am.* **81**, 1625–1640.
Tsuneishi, Y. & Nakamura, K. 1970. Faulting associated with the Matsushiro swarm earthquakes. *Bull. Earthq. Res. Inst. Tokyo Univ.* **48**, 29–51.
Wakita, H., Fujii, N., Matsuo, S., Notsu, K., Nagao, K. & Takaoka, N. 1978. 'Helium Spots': caused by a diapiric magma from the upper mantle. *Science* **200**, 430–432.
Weaver, C. S. & Hill, D. P. 1979. Earthquake swarms and local crustal spreading along major strike-slip faults in California. *Pure & Appl. Geophys.* **117**, 51–64.
Yeats, R. S. 1983. Large-scale Quaternary detachments in Ventura Basin, southern California. *J. geophys. Res.* **88**, 569–583.